



**HAL**  
open science

## Integrated facies analysis, magnetic susceptibility and sea-level fluctuations in the Frasnian (Upper Devonian) of the NW Algerian Sahara

Abdessamed Mahboubi, Jean-Jacques Cornee, Raimund Feist, Pierre Camps, Catherine Girard

► **To cite this version:**

Abdessamed Mahboubi, Jean-Jacques Cornee, Raimund Feist, Pierre Camps, Catherine Girard. Integrated facies analysis, magnetic susceptibility and sea-level fluctuations in the Frasnian (Upper Devonian) of the NW Algerian Sahara. *Geological Magazine*, 2019, 156 (8), pp.1295-1310. 10.1017/S0016756818000626 . hal-02115461

**HAL Id: hal-02115461**

<https://hal.umontpellier.fr/hal-02115461v1>

Submitted on 4 Nov 2022

**HAL** is a multi-disciplinary open access archive for the deposit and dissemination of scientific research documents, whether they are published or not. The documents may come from teaching and research institutions in France or abroad, or from public or private research centers.

L'archive ouverte pluridisciplinaire **HAL**, est destinée au dépôt et à la diffusion de documents scientifiques de niveau recherche, publiés ou non, émanant des établissements d'enseignement et de recherche français ou étrangers, des laboratoires publics ou privés.

1  
2  
3 1 Integrated facies analysis, magnetic susceptibility, and sea-level fluctuations in the  
4 2 Frasnian (Upper Devonian) of the NW Algerian Sahara  
5  
6 3

7 4 ABDESSAMED MAHBOUBI\*, JEAN-JACQUES CORNEE†, RAIMUND FEIST\*,  
8 5 PIERRE CAMPS† & CATHERINE GIRARD\*  
9  
10 6

11 7 \* Institut des Sciences de l'Evolution, Université de Montpellier, CNRS, IRD, CC064,  
12 8 Place Eugène Bataillon, Montpellier Cedex 05 (France)

13 9 † Géosciences Montpellier, CNRS and Université de Montpellier, Place Eugène  
14 10 Bataillon, 34095 Montpellier Cedex 05 (France)  
15  
16 11

17 12 \*Corresponding author: (email: [jean-jacques.cornee@gm.univ-montp2.fr](mailto:jean-jacques.cornee@gm.univ-montp2.fr))  
18 13 Phone (+33 4 67 14 36 35)  
19  
20 14

21 15 **Abstract:** Changes in palaeoenvironment are comparatively investigated in two  
22 16 representative Frasnian sections of NW Algerian Sahara integrating sedimentology,  
23 17 magnetic susceptibility, and conodont biofacies. The Ben Zireg section is  
24 18 characterized by condensed, and ferruginous calcareous deposits, whereas in the  
25 19 South Marhouma section the sedimentation rate is high, dominated by muddy  
26 20 nodular limestones with several hypoxic shale intervals. In both sections, sediments  
27 21 were mostly emplaced on pelagic outer ramps below the limit of storm wave-base,  
28 22 evolving in time from proximal to distal setting.

29 23 Investigations on temporal evolution of facies and MS data permits a brought first  
30 24 estimate of the local sea-level trends to be made in north-western Algeria. These  
31 25 trends match the overall long-term rise of sea-level recognized worldwide from  
32 26 Frasnian Zone 5 onward. Outstanding positive excursions of the sea-level curve  
33 27 related to the *semichatovae* transgression as well as to the late Frasnian  
34 28 transgression prior to the Upper Kellwasser event can be established in this area.  
35 29 Whereas the sharp regression of sea-level at the Upper Kellwasser level can be  
36 30 confirmed with our data, no particular trend is depicted at the transition of conodont  
37 31 zones 11 to 12 where the presence of the Lower Kellwasser level has not been  
38 32 clearly recognised so far.  
39  
40 33

41 34 **Keywords:** Frasnian, Algerian Sahara, facies, magnetic susceptibility, sea-level  
42  
43  
44  
45  
46  
47  
48  
49  
50  
51  
52  
53  
54  
55  
56  
57  
58  
59  
60

1  
2  
3 35

## 1. Introduction

37 The Frasnian stage in the Late Devonian is outstanding in the occurrence of one of  
38 the major sea-level rises in the Paleozoic (Haq & Shutter 2008), which culminated in  
39 spreading of basinal anoxic waters that eventually triggered the global biotic turnover  
40 at the terminal Frasnian Upper Kellwasser Event (Hallam & Wignall 1999). This long-  
41 term eustatic rise was documented mainly in Laurussia (e.g. Johnson, Klapper &  
42 Sandberg, 1985; Johnson & Sandberg, 1988; Alekseev, Konokova & Nikishin, 1996;  
43 Narkiewicz, 1988), and in South China (Chen & Tucker 2003). On the African  
44 Gondwana margin, after preliminary records from the Moroccan Anti-Atlas (Wendt &  
45 Belka 1991), only one accurate sea-level curve was recently provided (Dopieralska,  
46 Belka, & Walczak, 2016).

47 In this contribution we focus on Late Devonian facies and sea level fluctuations in the  
48 Algerian Sahara, by integrating results from two representative Frasnian sections of  
49 different marine palaeoenvironmental settings: the South Marhouma section and the  
50 Ben Zireg section (Fig. 1a). Indeed, this area is still poorly known in comparison to  
51 time-equivalent North America and European regions. Analyses of lithofacies,  
52 magnetic susceptibility and conodont biofacies were performed to depict changes in  
53 the depositional environment and sea level through time. The main objective of this  
54 study is first to determine whether observed changes and trends occur concomitantly  
55 in different settings of the region, and, secondly, to propose a first order relative sea-  
56 level curve through the Frasnian that can be compared with data from other  
57 continental entities. As such it aims to compare fluctuations in sea level with those  
58 depicted by Dopieralska, Belka, & Walczak. (2016) in the neighboring Tafilalet region  
59 and with the global trends in North America (Johnson, Klapper & Sandberg, 1985;  
60 Johnson & Sandberg, 1988).

61

## 2. Geological setting

63 The Algerian Sahara is part of the North-Gondwana epicontinental margin between  
64 the Maghrebic Variscan belt to the North and the West African craton to the South  
65 (Fig. 1a). This domain was moderately affected by the Variscan deformation. The  
66 South Marhouma section is located in the intracratonic Ougarta basin that is  
67 bordered to the south by a Precambrian shield. This basin was a strongly subsiding  
68 trough filled with continental and marine Ordovician through Carboniferous

1  
2  
3 69 sediments, up to 10km in thickness and slightly deformed by Variscan compressional  
4 70 movements (Donzeau, 1974). In the northern part of the basin Upper Devonian  
5 71 deposits are well exposed. At least 75 m of Frasnian sediments are continuously  
6 72 outcropping in the South Marhouma section (coordinates: 29°57'31. 6"N,  
7 73 002°06'07.8"W) (Fig. 1b). The succession comprises mudrock deposits (shales and  
8 74 marls) containing argillaceous micritic nodules, and, at its top, black shales that  
9 75 correspond to the Upper Kellwasser horizon. Goniatites from this area were  
10 76 described by Petter (1952) & Göddertz (1987), trilobites by Feist, Mahboubi & Girard  
11 77 (2016) and ichnological analyses by Bendella & Ouali (2014). The first conodont  
12 78 research was conducted by Mahboubi & Gatovsky (2014). It revealed a rather  
13 79 moderate yield of often insignificant conodont elements (less than 10 conodonts per  
14 80 kg in most samples) preventing a fine-scaled biostratigraphy to be established.  
15 81 However, the presence of a restricted number of conodont zones, i.e. FZ 5, 11, 12  
16 82 and 13 were recognized with confidence, whereas zones 6-7 and 8-10 remain  
17 83 undifferentiated. Many dark shale intervals, notably at the base of the succession (FZ  
18 84 1-4?) and in the uppermost part, did not provide any conodonts. Presently we rely on  
19 85 these poor data that only permit an incomplete zonation to be established at  
20 86 Marhouma.

21 87 In contrast to the high sedimentation rates in the Ougarta trough, these were much  
22 88 lower in the Bechar region at some 300 km further to the N. Here, Upper Devonian  
23 89 deposits represent condensed carbonate successions punctuated by hiatuses  
24 90 (Weyant, 1988). The Frasnian succession is most complete in the Ben Zireg section  
25 91 (coordinates: 31° 54'39. 4" N, 001° 47' 58.8" W), on the steep southern flank of an  
26 92 acute anticlinal structure. Conodont based biostratigraphy revealed a late Givetian  
27 93 through early Frasnian hiatus, superseded by a complete sequence where all  
28 94 conodont zones from FZ 5 to the Frasnian-Famennian boundary were recognized  
29 95 (Mahboubi *et al.* 2015). At the top of the succession a marker bed of typical  
30 96 Kellwasser facies is developed. This zonation is used in in our present study.

31 97

### 32 98 **3. Material and Methods**

33 99 Samples of hard rock were collected in intervals ranging from 0.2 to 2 m, depending  
34 100 on the thickness of the soft shale intercalations. Forty and sixty thin-sections were  
35 101 prepared from rock samples both from the South Marhouma and Ben Zireg sections,  
36 102 in order to to analyze petrofacies and fabrics. Microfacies descriptions follow Dunham

1  
2  
3 103 (1962) for carbonate rocks and Schieber (1989) for black shales. The identified facies  
4 104 were interpreted and related to a depositional environment setting according to  
5 105 Wright & Burchette (1996), Flügel (2004) and Pas *et al.* (2013; 2014). Photographs  
6 106 were taken with an integrated Olympus digital camera and with a scanning electron  
7 107 microscope (JEOL 5600).

8 108 Magnetic susceptibility measurements were performed on 90 and 54 samples in the  
9 109 South Marhouma and Ben Zireg sections, respectively, for preliminary investigation.  
10 110 Various lithologies have been measured (shales, arenaceous and carbonate rocks).  
11 111 In the laboratory, samples were cleaned from iron coatings prior to weighting with a  
12 112 highly accurate balance (precision of 0.01g). Measurements were performed with a  
13 113 Bartington susceptibility meter (MS-2). The unit of measure is expressed in  $\times 10^{-7} \text{ m}^3$   
14 114  $\text{kg}^{-1}$ .  
15 115

## 116 **4. Results and interpretations**

### 117 **4.a. Lithostratigraphy**

#### 119 **4.a.1. Ben Zireg section**

120 The measured section is 26.6 m thick (Fig. 2). It includes five units (Units 1 – 5)  
121 extending from the middle Frasnian to the early Famennian (Mahboubi *et al.*, 2015).  
122 The succession is dominated by rhythmic fine-grained carbonates.

123 Unit 1 belongs to Frasnian Zone 5 (FZ 5) just above a depositional hiatus during the  
124 early Frasnian. This Unit is characterized by ochre, sometimes brecciated, cherty  
125 beds with convolute-lamination (Fig. 3a). Thin iron-hydroxide coatings are displayed  
126 at the top of the unit.

127 Unit 2 belongs to FZ 6. It consists of greyish to brownish massive limestone beds,  
128 centimeters to decimeters in thickness, intercalated by mm to cm thick argillaceous  
129 limestone beds that display discrete nodular structures (Fig. 3b).

130 Unit 3 belongs to the interval ranging from FZ 7 to the top of FZ 11. It is characterized  
131 by well-bedded ferruginous and argillaceous limestones frequently coated by  
132 hardground films. The limestone beds are often wackstone with abundant pelagic  
133 microfauna (tentaculites and entomozoan crustaceans) associated with sparse  
134 euhedral pyrites and some phosphate grains. The amount of nodular structures

1  
2  
3 135 increases progressively upward and they are mostly related to pressure-dissolution  
4 136 surfaces.

5  
6 137 Unit 4 belongs to FZ 12. It is characterized by yellowish, massive, pseudo-nodular,  
7  
8 138 clay-rich limestones sometimes interbedded with thin blackish shales. The limestones  
9  
10 139 are mudstone to wackstone with sparse pelagic bioclasts (Fig. 2). Some of them are  
11 140 slightly bioturbated.

12  
13 141 Unit 5 extends from FZ 13 to the early Famennian stage. It consists of greyish and  
14 142 pinkish nodular to pseudo-nodular limestones and interbedded argillaceous micrite  
15 143 yielding poor faunas, except some tentaculite and cephalopod fragments. In the  
16 144 upper part of the limestones are 30 cm thick laminated blackish shales overlain by 35  
17 145 cm thick laminated pinkish calcisiltites without fossils (Fig. 3c). The black shales  
18 146 represent the Upper Kellwasser horizon.  
19  
20  
21  
22  
23 147

#### 24 148 **4.a.2. Marhouma section**

25  
26 149 The Frasnian succession is approximately 75 m thick and includes four units (Units 1  
27 150 – 4). The base of this section cannot be precisely dated. Details concerning conodont  
28 151 contents and their biostratigraphic implications were presented in Mahboubi &  
29 152 Gatovsky (2014). In contrast to Ben Zireg, this section is dominated by monotonous  
30 153 shale deposits rich in carbonate nodules (Fig. 4).

31  
32 154 Unit 1 belongs to the FZ 1 – 4 intervals. It consists of dark shales (Fig. 3d) with rare  
33 155 nodular limestones.

34  
35 156 Unit 2 extends from the upper part of FZ 1 – 4 to the lower part of FZ 8 – 10. It is  
36 157 characterized by cm to dm thick, greyish to reddish, pseudo-nodular to nodular  
37 158 bioclastic limestones (Fig. 3e), which alternate with unfossiliferous greyish to blackish  
38 159 shales. The limestones are wackestone with *Styliolina* (tentaculites) coquinas; they  
39 160 yield phacopid trilobites and cephalopods (*Mesobeloceras* sp.) on the surface of bed  
40 161 MH9 (Feist, Mahboubi & Girard, 2016).

41  
42 162 Unit 3 belongs to the FZ 8 – 10 to FZ 13 interval. It is characterized by unfossiliferous  
43 163 greenish and darkish shales with frequent reddish and greenish argillaceous nodular  
44 164 limestones (Fig. 3f). Toward the top, input of siliciclastic material increases, including  
45 165 mm thick intercalations of sandstone with planar-laminations. The Upper Kellwasser  
46 166 horizon of this section is marked by plane-laminated shales (Fig. 3g).  
47  
48  
49  
50  
51  
52  
53  
54  
55  
56  
57  
58  
59  
60

1  
2  
3 167 Unit 4 belongs to the early Famennian. It is mainly composed of dm thick diagenetic  
4 168 blackish argillaceous nodular limestones displaying large orthoceratids and  
5 169 brachiopods, and of unfossiliferous greyish laminated shales (Fig. 3h).  
6  
7  
8 170

#### 9 171 **4. b. Facies**

10  
11 172 On the basis of differences in texture, fossil components, and lithological nature,  
12 173 seven sedimentary facies are identified (Figs. 2, 4). The original texture of most rocks  
13 174 has been obscured or obliterated during burial diagenesis, tectonic processes, or  
14 175 both. Indeed, micro-shear zones and stylolithes are sometimes identified within  
15 176 nodular limestones. Moreover, the original texture (micrite) was transformed into  
16 177 microsparite.

17  
18 178 The facies description follows the distal to proximal order, from Facies 1 to Facies 7.  
19  
20  
21 179

22  
23  
24 180 **Laminated-black shales (F1):** In both sections, finely laminated black shales are  
25 181 interbedded with silty shales, calcareous shales, or both. Bed thicknesses range from  
26 182 centimeter to few meters. In the South Marhouma section, thick layers of black  
27 183 shales also display *septaria* nodules, whereas such shales are less common at Ben  
28 184 Zireg. The faunal content is represented only by poorly preserved shelly pelagic  
29 185 organisms (e.g. tentaculites).

30  
31 186 Shales, such as those at the base of Marhouma section (Fig. 3d), are usually  
32 187 interpreted as deposited in deep basin settings (e.g. Boulvain *et al.* 2004), probably  
33 188 below the storm wave-base. This facies is very common in North Africa (e.g. Ahnet  
34 189 and Mouydir basins (Wendt *et al.* 2006), with a high accumulation of organic matter  
35 190 (Boote, Clarke-Lowe & Traut, 1998). They are considered as the deepest facies in the  
36 191 Frasnian interval.  
37  
38  
39  
40  
41  
42  
43  
44  
45

46 192  
47 193 **Lithoclastic floatstone (F2):** The lithoclasts mainly consist of chaotic, randomly  
48 194 organized angular to rounded limestone and cherty clasts (Fig. 5a, b). Carbonate  
49 195 clasts are composed of monomict, poorly sorted pelagic mudstones belonging to  
50 196 Facies 3 (see below). Lithoclasts are supported by a matrix composed of calcisiltite,  
51 197 clay, microsparite, and iron-hydroxide. The fossil components consist of rare pelagic  
52 198 ostracods (entomozoans) and tentaculite debris. Inverse grading in the lower part of  
53 199 some dm- thick beds are observed.  
54  
55  
56  
57  
58  
59  
60

1  
2  
3 200 This facies was assigned to seismo-turbidites by Mutti *et al.* (1984) or megaturbidites  
4 201 by Cook *et al.* (1972). In our case, this facies is restricted to Unit 1 in association with  
5 202 convolute bedding. It corresponds to debris flows into a distal pelagic domain. This  
6 203 facies may also correspond to gravitational deposits that formed under low  
7 204 sedimentation rates and unstable depositional conditions (Rossetti & Góes, 2000). F2  
8 205 is similar to facies described elsewhere in the Upper Devonian successions from the  
9 206 Eastern Anti-Atlas (Wendt & Belka 1991). Convolute structures associated with  
10 207 reworked lithoclasts can be generated by seismic shocks giving rise to downslope  
11 208 movements (Spalletta & Vai 1984).  
12  
13  
14  
15  
16  
17  
18  
19

20 210 **Poorly fossiliferous mudstone (F3):** In the two sections, this facies is well  
21 211 represented. In the Marhouma section F3 is found in Units 1 and 3 consisting of  
22 212 greyish nodular cm-thick beds in shales. In the Ben Zireg section it occurs mainly in  
23 213 Units 3 and 5 as centimeter-thick fine-grained limestone beds or greyish nodular  
24 214 limestones, respectively. The matrix of this facies is micrite or microsparite. Micritic  
25 215 limestones lack bioturbation fabrics, whereas burrowing traces are sometimes  
26 216 observed in nodular limestones embedded within greyish shales. F3 is characterized  
27 217 by poor faunal content that is represented by pelagic organisms such as tentaculites,  
28 218 pelagic molluscs, entomozoans, and radiolarians. No current fabrics have been  
29 219 macroscopically observed in this facies.

30  
31  
32  
33  
34  
35  
36 220 The fine-grained matrix and rare fossils suggest low energy and open marine  
37 221 conditions, remaining probably under the storm wave-base (Pas *et al.*, 2013; 2014a).  
38 222 The scarcity of biogenic activities (e.g. borings and burrows) could reflect oxygen-  
39 223 depleted waters (Flügel, 2004). Nodules are often of late diagenetic origin, and were  
40 224 presumably produced in a deep burial diagenetic environment (James & Choquette  
41 225 1990).  
42  
43  
44  
45  
46  
47

48 227 **Argillaceous pelagic wackstone (F4):** This facies occurs mainly in middle Frasnian  
49 228 strata in both sections. It comprises cm- to dm- thick greyish to reddish limestones.  
50 229 Pressure solution processes commonly triggered tectonic stylolithisation. The  
51 230 common type of texture is wackstone with microbioclasts occurring in a patchily  
52 231 distribution. Thus, the matrix displays ferruginous blisters organized into isolated or  
53 232 grouped, concentric internal structures. The faunal content is commonly high, with  
54 233 tentaculites as the dominating organisms followed by entomozoans, radiolarians,  
55  
56  
57  
58  
59  
60



1  
2  
3 234 cephalopods, and pelagic mollusks (Fig. 5d). Additionally, scarce benthic faunas are  
4 235 represented by debris of trilobites, brachiopods, and ostracods. Bioclasts are  
5 236 generally poorly sorted; sometimes they are concentrated into mm-thin laminations  
6 237 with a random distribution of fossils and they are partially affected by bioturbation.

7  
8 238 On the basis of the abundance of pelagic assemblages, facies F4 is interpreted as  
9 239 deposited in a deep-water environment, likely just below the storm wave-base (*Pas et*  
10 240 *al.*, 2013; 2014a). Finely laminated biogenic detritus is interpreted as being deposited  
11 241 by turbidity currents or distal tempestites (*sensu* Aigner, 1985).  
12  
13  
14  
15  
16  
17

18 243 **Diversified mudstone to wackstone (F5):** This facies is mostly found in the  
19 244 uppermost part of both sections. In the South Marhouma section, it is composed of  
20 245 large dark diagenetic nodules of early *triangularis* Zone age. In the Ben Zireg section,  
21 246 the same facies occurs within greyish nodular muddy limestones. Fossil components  
22 247 are dominated by nektonic faunas such as cephalopods with *Orthoceras*, mostly  
23 248 fragmented and poorly preserved (Fig. 5c). Pelagic organisms, radiolarians,  
24 249 entomozoans, and tentaculites, are less frequent. Benthic faunas are more abundant  
25 250 compared with Facies 4 (Fig. 5e); they are dominated by ostracods, skeletal debris of  
26 251 echinoderms, brachiopods, and trilobites. This facies is locally bioturbated. Early  
27 252 diagenetic geopetal fillings are recognized within some rotated ostracods and  
28 253 cephalopods coquinas.

29  
30  
31  
32  
33  
34  
35  
36 254 In light of the increase in benthic faunal diversity, which is a striking feature of zones  
37 255 with normal oxygen concentration (Flügel, 2004), the depositional setting of this  
38 256 facies might be located above storm wave-base.  
39  
40  
41

42 257

43 258 **Lime ostracod mudstone (F6):** This facies is not frequent in the studied sections  
44 259 (samples BZ10a, BZ11, BZ13a, and MH6'). It occurs mostly in FZ 12 in the Ben Zireg  
45 260 section. It consists of yellowish thin bedded argillaceous limestones. The matrix is  
46 261 microsparite to sparite, rarely containing euhedral replacement of dolomite crystals.  
47 262 The bioclastic components of this mudstone consist predominantly of benthic  
48 263 ostracods (Fig. 5f) followed by trilobite and brachiopod fragments. Additionally,  
49 264 pelagic elements are limited to entomozoans, radiolarians, and unrecognized pelagic  
50 265 shell fragments. Micritic geopetal infillings are sometimes observed. The systematic  
51 266 study of benthic ostracods from acid residues revealed the presence of the suborders  
52  
53  
54  
55  
56  
57  
58  
59  
60

1  
2  
3 267 Podocopida and Metacopida that can be related to the Assemblage III of Casier  
4 268 (2008).

5  
6 269 The abundance of the ostracod assemblage might indicate a more proximal  
7  
8 270 depositional setting compared with the previous environment, likely below the fair  
9  
10 271 weather wave-base. The frequent occurrence of disarticulated ostracods may  
11 272 suggest para-autochthonous aggregations produced by episodic storm-induced sea  
12 273 floor disturbances (Schülke & Popp, 2005).

14  
15 274

16 275 **“Microbial (?) shale” (F7):** This facies is common in "restricted" environments in the  
17  
18 276 latest Frasnian. It is exhibited in the South Marhouma section as lenticular cm- to dm-  
19 277 thick darkly carbonaceous to silty shale. The texture is close to the striped shale  
20 278 facies of Schieber (1989), with silt and mud couplets (light) alternating with  
21 279 carbonaceous silty shale (dark) (Fig. 6f). In petrographic thin section, the texture  
22 280 displays discontinuous wavy-crinkly laminae of kerogenous matter that are widely  
23 281 associated with framboïdal pyrites and cubic euhedral crystals (Figs. 6b, c, e). Also,  
24 282 terrigenous quartz grains and isolated mud fragments can be found. Imbricated flat  
25 283 pebbly conglomerates with argillaceous clasts are observed in bed MH26bas (Fig.  
26 284 6a). Characteristic organisms are reworked benthic ostracods, rare brachiopods, and  
27 285 undetermined mollusk shells.

28  
29 286 In the Ben Zireg section, the microbial (?) shale facies is observed in bed BZ15D  
30 287 (Uppermost FZ 13). It consists of pink laminated calcareous silty shale. The thin  
31 288 sections display a fine-grained matrix with abundant dolomite crystals and rare mica  
32 289 crystals. The wavy-crinkly laminae described above are less common (Fig. 6e) and  
33 290 organized into fine kerogenous units alternating with fine-grained calcareous  
34 291 laminae. SEM observations display tube-like shapes (Fig. 6d) occasionally forming  
35 292 ramiform structures and sometimes associated with rare framboïdal pyrites. Fossils  
36 293 are very sparse, with brachiopods, benthic ostracods and tentaculite fragments.

37  
38 294 Framboïdal pyrite is commonly present in hypoxic to anoxic environments (e.g. Li  
39 295 Tian *et al.* 2014; Peckmann & Thiel 2004; Wignall, Newton & Brookfield, 2005) where  
40 296 crystallization is partly controlled by bacterial activity (e.g. Folk, 2005; Mac Lean *et*  
41 297 *al.*, 2008). The association of wavy to wavy-crinkly structures with kerogen laminae  
42 298 has been considered resulting from the occurrence of benthic microbial  
43 299 (cyanobacterial?) mats (e.g. Schieber, 1986, 1989; Sur *et al.*, 2006; Deb, Schieber &  
44 300 Chaudhuri, 2007) and coccoidal bacteria have been identified within such deposits

1  
2  
3 301 (Kaźmierczak, Kremer & Racki, 2012). Even if no obvious diagnostic feature of  
4 302 primary cyanobacterial mats (e.g. web-like texture indicator of benthic coccoidal  
5 303 remnants, Kremer & Kaźmierczak, 2005) were found in the studied sections, the  
6 304 presence of organic matter, framboidal pyrite, wavy lamination, wavy lenticular  
7 305 lamination with shale fragments, wavy crinkly structure and tubular structures (SEM)  
8 306 are strongly suggestive of the presence of microbial mats acting during the deposition  
9 307 of the black shales in the two sections. The presence of mud and silt couplets with  
10 308 locally reworked fossils and mixing of conodont assemblages indicate episodic high  
11 309 energy episodes attributed to storms. Such an interpretation is compatible with that of  
12 310 Schieber (1986, 1989) who located the depositional environment of similar shales  
13 311 between fair weather wave-base and average storm wave-base.  
14  
15  
16  
17  
18  
19  
20  
21  
22

#### 23 313 **4.c. Magnetic susceptibility trends**

24 314 First application of the magnetic susceptibility (MS) technique (Figs. 8, 9) provided  
25 315 extremely low MS values for the Frasnian and basal Famennian strata. These vary  
26 316 between  $0.1 \times 10^{-7} \text{ m}^3 \text{ kg}^{-1}$  and  $8 \times 10^{-7} \text{ m}^3 \text{ kg}^{-1}$  at the south Marhouma section with an  
27 317 empirical average value of  $1.9 \times 10^{-7} \text{ m}^3 \text{ kg}^{-1}$ . They are even lower in the Ben Zireg  
28 318 anticline where they fluctuate between  $3.7 \times 10^{-7} \text{ m}^3 \text{ kg}^{-1}$  and  $0.4 \times 10^{-7} \text{ m}^3 \text{ kg}^{-1}$  with  
29 319 an average of  $1.3 \times 10^{-7} \text{ m}^3 \text{ kg}^{-1}$ . Even if the reliability of the MS measures should be  
30 320 tested by additional magnetic techniques (Da Silva *et al.*, 2013) to appreciate  
31 321 problems of re-magnetization or diagenesis, the mean values are compatible with  
32 322 those from other Frasnian sites. In both Algerian sections the averages of MS values  
33 323 are lower than those for the  $\text{MS}_{\text{marine standard}}$  ( $5.5 \times 10^{-7} \text{ m}^3 \text{ kg}^{-1}$ ) of Ellwood *et al.* (2011)  
34 324 and (Da Silva, Mabile & Boulvain, 2009). This was also observed in the Carnic Alps  
35 325 (Pas *et al.*, 2014a) and in the Dinant Synclinorium (Pas *et al.*, 2014b) where mean  
36 326 values range from 0.1 to  $1 \times 10^{-7} \text{ m}^3 \text{ kg}^{-1}$ .

37  
38  
39  
40  
41  
42  
43 327 Qualitative analysis of the magnetic susceptibility suggests the same global trend  
44 328 with shared peaks, which are considered as isochronous (Crick *et al.* 2002), in the  
45 329 South Marhouma and in Ben Zireg sections (Figs. 8, 9). At Marhouma, the lower part  
46 330 of the section from FZ1-4 to FZ6-7 shows important fluctuation of MS value from 0 to  
47 331  $8 \times 10^{-7} \text{ m}^3 \text{ kg}^{-1}$ . The upper part of the section, from FZ8-10 to Famennian, shows low  
48 332 values between 0 and  $3 \times 10^{-7} \text{ m}^3 \text{ kg}^{-1}$ . At Ben Zireg, the lower part of the section  
49 333 from FZ5 to FZ7 shows little fluctuation, between 0 and  $3 \times 10^{-7} \text{ m}^3 \text{ kg}^{-1}$ . In the upper  
50  
51  
52  
53  
54  
55  
56  
57  
58  
59  
60

1  
2  
3 334 part of the section, from FZ8-10 to Famennian, the MS value remains low, between 0  
4 335 and  $1 \times 10^{-7} \text{ m}^3 \text{ kg}^{-1}$ .

5  
6 336

## 7 8 337 **5. Discussion**

9 338

### 10 339 **5.a. Local depositional environment**

11 340 Paleoenvironmental interpretations of depositional settings of Facies 1 and 3 to 7  
12 341 observed in both sections (plus F2 at Ben Zireg only) allow proposing that the  
13 342 sediments were deposited along a low angle, mid to outer ramp profile *sensu* Wright  
14 343 & Burchette (1996) at regional scale (Fig. 7).

15  
16 344

#### 17 345 **5.a.1. Ben Zireg section**

18 346 The section is dominated by fine grained carbonates above a major gap in the lower  
19 347 Frasnian. This gap corresponds to a non-deposition and erosion? in submarine  
20 348 setting and was related elsewhere to bottom currents (Hüneke, 2006). The presence  
21 349 of such currents has not been evidenced at Ben Zireg. An outer ramp model is  
22 350 suggested for this area at the northern margin of Algerian Sahara (Fig. 7). In this  
23 351 model the deepest deposits are represented by some black shale intervals (Facies 1,  
24 352 Fig. 2 and 3d) and siliceous deposits with convolutes and breccias (Facies 2; Figs.  
25 353 3a, 5a, b). In our model (Fig. 7), Facies 4 and 5 were emplaced below storm wave-  
26 354 base, as no current features were found. In Facies 4 the presence of submicrometric  
27 355 hydroxides may result from iron - bacteria activity (Mamet & Préat 2006). Common  
28 356 hardgrounds point to repeated episodes of cementation on the sea floor. The  
29 357 proximal part of the ramp displays accumulations of fragmented bioclasts from both  
30 358 benthic and pelagic communities. This is interpreted as indicating a deposition  
31 359 between storm wave-base and fair-weather wave-base, with an increasing amount of  
32 360 benthic fauna upward from Facies 5 to Facies 7 indicative of a shallowing upward  
33 361 trend.

34  
35 362

#### 36 363 **5.a.2. South Marhouma section**

37 364 The section is dominated by mudrocks (e.g. shales) and fine-grained carbonate  
38 365 deposits with open marine fauna.

1  
2  
3 366 From FZ 1 to 4 sedimentation resumed in autochthonous facies 1 and 3 which are the  
4 367 deepest facies. Facies 1 (black shales) probably indicates dysoxic to anoxic bottom  
5 368 conditions. Facies 2 was not found (Fig. 8). From FZ5 to FZ13 the nodular  
6 369 argillaceous limestones (Facies 3) with mudstone texture and rare fauna suggest  
7 370 distal depositional setting under quiet depositional conditions. The fine-grained  
8 371 bioclastic mudstone and wackstone (Facies 4 and Facies 5) with overwhelming  
9 372 abundance of open marine fauna (Facies 4) attest depositional setting similar to F1  
10 373 and F3 but with some influence of shallow-water. Frequent occurrences of dark  
11 374 shales in this setting may reflect confined conditions when only organic matter was  
12 375 deposited upon the substrate. A shallower ramp is recognized during FZ6 – 7 and  
13 376 FZ12 by the increase of benthic faunal components (Facies 5). The shallowest facies  
14 377 herein is depicted by the occurrence of microbial (?) benthic mats (Facies 7) that are  
15 378 affected by storm action below the fair weather wave-base.

16  
17  
18  
19  
20  
21  
22  
23  
24  
25  
26 379

### 27 380 **5.a.3. Comparison between both sections**

28 381 Stratigraphic correlation between Ben Zireg and Marhouma was documented in  
29 382 Mahboubi *et al.* (2015). The Frasnian deposits of the South Marhouma section are  
30 383 nearly three times thicker than those of Ben Zireg, though mostly represented by  
31 384 distal shaly deposits (Facies1). We conclude in a higher sedimentation rate under  
32 385 subsiding basinal conditions at Marhouma. In contrast, distal carbonate deposits with  
33 386 minor shaly interbeds characterize Ben Zireg where Facies 3 to Facies 5 dominate.  
34 387 We suggest a discrete submarine rise setting on an outer ramp under low  
35 388 sedimentation rates. Such a depositional setting results either from submarine rise  
36 389 topography, or from enhanced current activity, or from a more distant location to the  
37 390 source areas of detrital inputs.

38  
39  
40  
41  
42  
43  
44  
45 391 As a whole, the Frasnian interval at Marhouma is punctuated by several  
46 392 developments of hypoxic facies (black and grey shales) that are not identified in the  
47 393 Ben Zireg section. The absence of such facies is presumably due to the submarine  
48 394 rise topography or to currents activity or to a far distant location regarding the  
49 395 sources of detrital and biogenic materials magnetic susceptibility values are low, see  
50 396 below)..

51  
52  
53  
54  
55  
56 397

### 57 398 **5.b. Sea-level fluctuations**

58  
59  
60

1  
2  
3 399 Integrating both lithofacies and MS data (Figs. 8 and 9), as well as data of conodont  
4 400 biofacies (Seddon & Sweet, 1971; Sandberg, 1976; Klapper & Barrick, 1978;  
5 401 Sandberg & Ziegler 1979) 'recently published in both studied sections (Mahboubi &  
6 402 Gatowsky, 2014; Mahboubi *et al.*, 2015), we tentatively interpret environmental  
7 403 changes through middle and late Frasnian times in terms of bathymetrical variation.  
8 404 However, we are aware that changes in bathymetry might not be the sole cause of  
9 405 fluctuations in the percentage of conodont genera in succeeding populations (Belka  
10 406 & Wendt 1992).  
11  
12  
13  
14  
15  
16  
17

### 18 408 **5.b.1. Early Frasnian**

19 409 During the early Frasnian (FZ1 – 4), the Marhouma section displays a regressive  
20 410 trend with an upward change from facies 1 to 3 and fluctuating MS values (Fig. 8).  
21 411 This trend is in contradiction to the transgressive trend recorded in North America  
22 412 (Fig. 10) at that time. It could be related to the specific location of the Marhouma  
23 413 section where abundant fine-grained siliciclastic inputs from the emerging West  
24 414 African Shield might have obscured the eustatic signal.  
25  
26  
27  
28  
29  
30

### 31 416 **5.b.2. Middle Frasnian**

32 417 Between FZ 5 and the beginning of FZ 8/10, both sections display instabilities of MS  
33 418 and lithofacies values (Fig. 8 and 9). During this interval, at Marhouma, slight shifts of  
34 419 MS values roughly reflect concomitant shifts in lithofacies. In contrast, at Ben Zireg,  
35 420 shifts in both MS and lithofacies values, though discernible, are less pronounced with  
36 421 lower amplitudes in their maximum excursions. MS values, in particular, that vary  
37 422 between 0 and 8 units at Marhouma, are much lower at Ben Zireg with a shift from 1  
38 423 to 3 units and as such being almost insignificant. In parallel, variations in succeeding  
39 424 lithofacies are more vigorous with shifts from F1 to F6 at Marhouma, whereas these  
40 425 are restricted to F2+3 and F4 at Ben Zireg. Mean prevalence of F4 in both sections  
41 426 along with a poorly documented decrease in MS values coincide with biofacies  
42 427 indicators available at Ben Zireg that shift temporarily from shallower Po-Ic  
43 428 (*Polygnathus-Icriodus*) in FZ 6 to deeper Po between FZ 7 and the beginning of  
44 429 FZ8/10 before returning to Po-Ic thereafter (Mahboubi *et al.*, 2015).  
45  
46  
47  
48  
49  
50  
51  
52  
53  
54 430 During the middle Frasnian the global trend is transgressive (Johnson & Sandberg,  
55 431 1988; Sandberg *et al.*, 1992). In the nearby Tafilalt region this trend is perceptible  
56 432 since FZ8 (Dopieralska, Belka, & Walczak, 2016) and culminates at the end of FZ 10  
57  
58  
59  
60

1  
2  
3 433 (Fig. 10). This trend is likewise to be observed at Ben Zireg. At Marhouma, the  
4 434 global transgressive trend begins in the lower part of FZ6 to FZ10 but a marked  
5 435 regressive event occurred at the transition from during FZ6-7.  
6  
7  
8 436

### 9 437 **5.b.3. Late Frasnian**

10  
11 438 MS values remain constantly very low throughout the late Frasnian without any  
12 439 significant changes at the Upper Kellwasser level in particular.

13 440 During the early FZ11 there is a regressive event followed by a transgressive peak in  
14 441 the late FZ 11. This transgressive peak is characterized by a significant extension of  
15 442 deep sea lithofacies, associated with biofacies Po-Pa (*Polygnathus-Palmatolepis*)  
16 443 dominated conodont associations. This signal is most obvious at Ben Zireg  
17 444 (Mahboubi *et al.*, 2015), whereas, at Marhouma, the paucity of available conodont  
18 445 record prevents to confirm the slight deepening of the sedimentary setting there  
19 446 (Mahoubi & Gatowsky, 2014). The curve of Ben Zireg remarkably coincides with the  
20 447 curves obtained in Euramerica and in the Tafilalt (Fig. 10). At Marhouma, only the  
21 448 transgressive peak is clearly recorded. Dopieralska, Belka, & Walczak (2016)  
22 449 emphasize the importance of the *semichatovae* transgression with the highest  
23 450 positive shift in  $\epsilon\text{Nd}$  values within FZ 11. This event has earlier been described from  
24 451 Euramerica where it is characterized by the sudden spread of *Palmatolepis*  
25 452 *semichatovae* in FZ 11 (Sandberg *et al.* 1992; Sandberg, Morrow & Ziegler, 2002).  
26 453 This species has not been established in the studied sections, but the obvious  
27 454 transgressive episode recorded within FZ 11 at both Marhouma and Ben Zireg may  
28 455 most likely correspond to this event. As a whole, the *semichatovae* transgression is  
29 456 evidenced in the Saharian Platform.

30  
31  
32  
33 457 During FZ 12 shallower environments reappear between Facies 5 and Facies 6 at  
34 458 Ben Zireg, and between Facies 1 and Facies 7 at Marhouma. Biofacies in both  
35 459 sections clearly indicate a shallowing trend with predominance of Po-An (*Polygnathus-*  
36 460 *Ancyrodella*) (Mahoubi & Gatowsky, 2014; Mahboubi *et al.*, 2015). This regressive  
37 461 trend was also identified in Euramerica and in the Tafilalt (Fig. 10).

38  
39 462 At the top of FZ 12 and the transition between FZ 12 and FZ 13 the hypoxic Lower  
40 463 Kellwasser horizon (LKW), usually occurring elsewhere, is not developed in its typical  
41 464 shale facies in our sections. Litho- and biofacies indicate a sudden increase in  
42 465 bathymetry followed up by fluctuations of lithofacies that average increase of water  
43 466 depth up to the Upper Kellwasser (UKW) horizon. Indicators of concomitant biofacies  
44  
45  
46  
47  
48  
49  
50  
51  
52  
53  
54  
55  
56  
57  
58  
59  
60

1  
2  
3 467 appear to be somewhat contradictory, as they remain constant in prevalence of Pa-  
4 468 Po and Pa at Ben Zireg but return to shallower signals at Marhouma (Mahboubi &  
5 469 Gatovsky 2014, Mahboubi *et al.* 2015). The increase in bathymetry observed in our  
6 470 sections is in accordance with that of Euramerica and Tafilalt (Fig. 10). Dopieralska,  
7 471 Belka, & Walczak (2016) also identified regressive trends coinciding in particular with  
8 472 the Lower and Upper Kellwasser extinction events at the FZ 12/13 transition and at  
9 473 the top of FZ 13 respectively. At Ben Zireg and Marhouma the LKW deposits are not  
10 474 lithologically recognized and precisely located; any regressive trend occurs slightly  
11 475 earlier, still within FZ12 when biofacies Po-An (*Polygnathus-Ancyrodella*) biofacies  
12 476 dominates. This anomaly might perhaps be introduced by local palaeoecological  
13 477 factors, in relation to the absence of the Lower Kellwasser horizon, as thereafter  
14 478 “normal” transgressive conditions are progressively emplaced matching the global  
15 479 sea-level trend.

16 480 The Upper Kellwasser horizon is characterized by its typical hypoxic facies at Ben  
17 481 Zireg. Bathymetric criteria point to a relative highstand of sea-level at the beginning of  
18 482 the event followed up by a marked decrease of water depth until its top with  
19 483 development of Pa-An biofacies (Mahboubi *et al.*, 2015) and occurrence of possible  
20 484 “microbial shales” (F7). In contrast, at Marhouma, the drop in sea level seems to start  
21 485 earlier when F7 and Po-Ic (*Polygnathus-Icriodus*) are present at the beginning of the  
22 486 presumed Upper Kellwasser (Mahboubi & Gatovsky, 2014). Consequently, it cannot  
23 487 be excluded that the equivalent of the Upper Kellwasser event starts a little earlier at  
24 488 Marhouma than considered by Mahboubi & Gatovsky (2014). At top of FZ 13 the  
25 489 major regression during the UKW event occurs both at Ben Zireg and Marhouma and  
26 490 is in accordance with the results of Dopieralska, Belka, & Walczak (2016) and  
27 491 Johnson & Sandberg (1988).

28 492

#### 29 493 **5.b.4. Summary**

30 494 The bathymetric curves in the Saharian Platform display a continuing sea-level rise  
31 495 through the middle Frasnian punctuated by a first regression at the base of FZ11,  
32 496 but with a minor regression at FZ6 at Marhouma. During the late Frasnian in  
33 497 Euramerica, this global transgressive event achieves its highest stand from the top of  
34 498 FZ 11 to FZ 13, intercalated by two regressions prior to and succeeding the Lower  
35 499 Kellwasser (LKW) event. This is matched by the recently established curve based on  
36 500 Nd isotopic data presented by Dopieralska, Belka, & Walczak (2016). Coincident



1  
2  
3 501 results on bathymetric evolution obtained by an independent method, data gathered  
4 502 from neighboring southeastern Moroccan terrains, are of importance for the  
5 503 comparative interpretation of the curve established in SW Algeria (Fig. 10).

6  
7  
8 504 As expected, Frasnian sections of SW Algeria display a similar sea-level evolution  
9 505 through mid- and late Frasnian times than in neighboring parts of Gondwana  
10 506 (Morocco). Differences in deposits (absence or presence of LKW), in timing (changes  
11 507 in sea-level occurring later in SW Algeria than elsewhere) and amplitude of changes  
12 508 in both litho- and biofacies between sites might result from effects of locally different,  
13 509 tectonically driven rates in subsidence. In addition, sampling bias cannot be excluded  
14 510 in highly condensed portions such as in the lower part of the Ben Zireg section, or, on  
15 511 the contrary, when conodonts are rather scarce in deposits with high sedimentation  
16 512 rates as occur in the early through middle Frasnian in the Marhouma trough  
17 513 (Mahboubi *et al.*, 2015).

18  
19  
20  
21  
22  
23  
24  
25  
26 514

## 27 515 **6. Conclusions**

28 516 The investigated sections through the middle and late Frasnian are composed of  
29 517 seven marine lithofacies that vary in time and duration throughout the successions.  
30 518 These lithofacies are organized along a very low angle, mid to outer ramp at the  
31 519 scale of the western part of the Saharian platform. Condensed carbonate  
32 520 sedimentation on discrete highs prevail in the North (Ben Zireg) whereas abundant  
33 521 shaly deposits occur in the South (Marhouma). Vertical facies changes are most  
34 522 perceptible at Marhouma both during the early middle and the latest Frasnian where  
35 523 rapid shifts between deep and shallow lithofacies occur. During the late middle and  
36 524 early upper Frasnian more stable conditions with the deposition of bioclastic mud-  
37 525 and wackstones prevail. Conversely, at Ben Zireg, these latter conditions  
38 526 characterize the condensed middle and earliest late Frasnian succession. A  
39 527 deepening occurred in the upper part of FZ 11, followed up by a marked shallowing  
40 528 at the beginning of FZ 12 and an average deepening up to the Upper Kellwasser.  
41 529 The latter is marked in both sections by a regressive-transgressive cycle.

42  
43  
44  
45  
46  
47  
48  
49  
50  
51 530 Provisional measurements of magnetic susceptibility provided very low values. Shifts  
52 531 are more pronounced with rapid variations in the lower part of the middle Frasnian,  
53 532 remaining constantly rather low thereafter up to the Frasnian/Famennian boundary in  
54 533 both sections. In particular, no significant shift is available at the equivalent levels of  
55  
56  
57  
58  
59  
60

1  
2  
3 534 the Kellwasser event. Further, more detailed and bed-by-bed measurements are  
4 535 necessary to reconsider MS trends comparatively.

5 536 A sea-level curve, tentatively established mainly on data from Ben Zireg matches the  
6 537 “standard” curves already provided at a world scale. Especially, the middle Frasnian  
7 538 transgression, the lower FZ11 regression, the *semichatovae* transgression within FZ  
8 539 11, the lower FZ12 regression, the upper FZ13 transgression and Upper Kellwasser  
9 540 regression are clearly evidenced in the Saharian platform.

10  
11  
12  
13 541

14  
15  
16 542 **Acknowledgements**

17  
18  
19 543 Algerian authorities are thanked to provide permission to access to the field. We  
20 544 acknowledge Tadjedinne Hassen, Kada Abess and Brigitte Meyer-Berthaud for their  
21 545 help in the field. The first field trip was supported by the ANR Palasiafrica (ANR-08-  
22 546 JCJC-0017). A. Mahboubi is grateful to Jean-Louis Bodinier for his funding (IRSES  
23 547 MEDYNA grant) for one month. This is publication ISE-M 2017-XXX.

24  
25  
26  
27 548  
28  
29  
30  
31  
32  
33  
34  
35  
36  
37  
38  
39  
40  
41  
42  
43  
44  
45  
46  
47  
48  
49  
50  
51  
52  
53  
54  
55  
56  
57  
58  
59  
60

549 **References**

- 550 AIGNER, T. 1985. Storm Depositional Systems. Dynamic Stratigraphy in Modern and  
551 Ancient Shallow-Marine Sequences. Springer-Verlag, Berlin, *Lecture Note in Earth*  
552 *Sciences* **3**, 1-174
- 553 ALEKSEEV, A.S., KONONOVA L.I., NIKISHIN A.M. 1996. The Devonian and  
554 Carboniferous of the Moscow Syncline (Russian Platform): stratigraphy and sea-  
555 level changes. *Tectonophysics* **268**, 149-168.
- 556 BECKER, R.T., GRADSTEIN, F.M & HAMMER, O. 2012. The Devonian Period. In  
557 *The geologic time scale 2012* (eds Gradstein, F., Ogg, J., Schmitz, M. & Ogg, G.),  
558 Elsevier, 559-601.
- 559 BELKA, Z. & WENDT, J. 1992. Conodont biofacies pattern in the Kellwasser Facies  
560 (upper Frasnian/lower Fammenian) of the eastern Anti-Atlas, Morocco.  
561 *Palaeogeography, Palaeoclimatology, Palaeoecology* **91**, 143-173
- 562 BENDELLA, M. & MEHADJI, A.O. 2014. Depositional environment and Ichnology  
563 (Nereites ichnofacies) of the Late Devonian Sahara region (SW Algeria). *Arabian*  
564 *Journal of Geology* **7**, 1-14.
- 565 BOOTE, D.R.D., CLARK-LOWES, D.D. & TRAUT M.W. 1998. Palaeozoic petroleum  
566 systems of North Africa. In *Petroleum Geology of North Africa* (eds D.S.  
567 Macgregor, R.T.J. Moody & D.D. Clark-Lowes). Journal of the Geological Society  
568 of London, Special Publication **132**, 7-68.
- 569 BOULVAIN, F. , CORNET, P., DA SILVA, A.C., DELAITE, G., DEMANY B.,  
570 HUMBLET, M., RENARD, M. & COEN-AUBERT, M. 2004. Reconstructing atoll-  
571 like mounds from the Frasnian of Belgium. *Facies* **50**, 313–326.
- 572 CASIER, J.C. 2008. Résumés des communications et guide de l'excursion  
573 consacrée aux ostracodes du Dévonien Moyen et Supérieur de Dinant. In *22<sup>th</sup>*  
574 *Réunions des Ostracologistes de Langue Française*, Institut Royal des Sciences  
575 Naturelles de Belgique, Département de Paléontologie, Bruxelles, pp 1-88.
- 576 CHEN, D. & TUCKER, M.E. 2003. Palaeokarst and its implication for the extinction  
577 event at the Frasnian–Famennian boundary (Guilin, south China). *Journal of the*  
578 *Geological Society of London* **161**, 895-898.
- 579 COOK, H.E., MCDANIEL, P.N., MOUNTJOY, E.W. & PRAY, L.C. 1972.  
580 Allochthonous carbonate debris flows at Devonian bank ("reef") margins, Alberta,  
581 Canada. *Bulletin of Canadian Petroleum Geology* **20**, 439–497.

- 1  
2  
3 582 CRICK, R.E., ELLWOOD, B.B., HLADIL, J., EL HASSANI, A., HROUDA, F. &  
4 583 CHLUPAC, I. 2001. Magnetostratigraphy susceptibility of the Pridolian–Lochkovian  
5 584 (Silurian–Devonian) GSSP (Klonk, Czech Republic) and coeval sequence in Anti-  
6 585 Atlas Morocco. *Palaeogeography, Palaeoclimatology, Palaeoecology* **167**, 73-  
7 586 100.
- 8 587 DA SILVA, A. C., DE VLEESCHOUWER, D. et al. 2013. Magnetic susceptibility as a  
9 588 high-resolution correlation tool and as a climatic proxy in Paleozoic rocks-merits  
10 589 and pitfalls: examples from the Devonian in Belgium. *Marine and Petroleum*  
11 590 *Geology* **46**, 173-189.
- 12 591 DA SILVA, A.C., MABILLE, C. & BOULVAIN, F. 2009. Influence of sedimentary  
13 592 setting on the use of magnetic susceptibility: examples from the Devonian of  
14 593 Belgium. *Sedimentology* **56**, 1292-1306.
- 15 594 DEB, S.P., SCHIEBER, J. & CHAUDHURI, A.K. 2007. Microbial mat features,  
16 595 mudstones of the Mesoproterozoic Somanpalli Group, Pranhita-Godavari Basin,  
17 596 India. In *Atlas of Microbial Mat Features Preserved within the Siliciclastic Rock*  
18 597 *Record* (eds Schieber, J., Bose, P.K., Eriksson, P.G., Banerjee, S., Jadavpur,  
19 598 S.S., Altermann, W. & Catuneanu, O.). Elsevier, Amsterdam, **2**, 171-180.
- 20 599 DONZEAU, M. 1974. L'arc Anti-Atlas-Ougarta (Sahara Nord occidental, Algérie,  
21 600 Maroc). *Comptes Rendus de l'Académie des Sciences, Paris, (II)*, **278**, 417-420.
- 22 601 DOPIERALSKA, J., BELKA, Z. & WALCZAK, A. 2016. Nd isotope composition of  
23 602 conodonts: An accurate proxy of sea-level fluctuations. *Gondwana Research* **34**,  
24 603 284-295.
- 25 604 DUNHAM, R.J. 1962. Classification of carbonate rocks according to depositional  
26 605 texture. In *Classification of Carbonate Rocks* (ed Ham, W.E.). American  
27 606 Association of Petroleum Geologists, Memoir **1**, 108-121.
- 28 607 ELLWOOD, B.B., TOMKIN, J.H., EL HASSANI, A., BULTYNCK, P., BRETT, C.E.,  
29 608 SCHINDLER, E., FEIST, R. & BARTHOLOMEW, A.J. 2011. A climate-driven  
30 609 model and development of a floating point time scale for the entire Middle  
31 610 Devonian Givetian Stage: A test using magnetostratigraphy susceptibility as a  
32 611 climate proxy. *Palaeogeography, Palaeoclimatology, Palaeoecology* **304**, 85-95.
- 33 612 FEIST, R., MAHBOUBI, A. & GIRARD, C. 2016. New Late Devonian phacopid  
34 613 trilobites from Marhouma, SW Algerian Sahara, *Bulletin of Geosciences* **91**, 243-  
35 614 259.

- 1  
2  
3 615 FLÜGEL, E. 2004. *Microfacies of carbonate rocks. Analysis, Interpretation and*  
4 616 *Application*. Springer-Verlag , Berlin, Heidelberg, NewYork, pp 1-984.
- 5  
6 617 FOLK, R.L., 2005. Nannobacteria and the formation of framboidal pyrite: Textural  
7 618 evidence. *Journal of Earth Systems in Sciences* **114**, 369-374.
- 8  
9 619 GÖDDERTZ, B. 1987. Devonische Goniatiten aus SW-Algerien und ihre  
10 620 stratigraphische Einordnung in die Conodonten-Abfolge. *Palaeontographica*  
11 621 *Abteilung A* **197**:127-220.
- 12  
13 622 HALLAM, A. & WIGNALL, P.B. 1999. Mass extinctions and sea-level changes. *Earth*  
14 623 *Science Review* **48**, 217-250.
- 15  
16 624 HAQ, B.U. & SCHUTTER, S.R. 2008. A Chronology of Paleozoic Sea-Level  
17 625 Changes. *Science* **322**, 64-68.
- 18  
19 626 JAMES, N.P. & CHOQUETTE, P.W. 1990. Limestone - The meteoric diagenetic  
20 627 environment. In *Diagenesis* ( eds Mc Ilreath, I.A. & Morrow, D.W.). *Geosciences*  
21 628 *Canada* **4**, 35-73.
- 22  
23 629 JOHNSON, J. G., KLAPPER, G. & SANDBERG, C. A.1985. Devonian eustatic  
24 630 fluctuations in Euramerica. *Geological Society of America Bulletin* **96**, 567-87.
- 25  
26 631 JOHNSON, J.G. & SANDBERG, C.A. 1988. Devonian eustatic events in the Western  
27 632 United States and their biostratigraphic responses. In *Devonian of the World* (eds  
28 633 McMillan, N.J., Embry, A.F. & Glass, D.J.). *Canadian Petroleum Geology, Calgary*  
29 634 **14**,171-178.
- 30  
31 635 KAŻMIERCZAK, J., KREMER, B. & RACKI, G., 2012. Late Devonian marine anoxia  
32 636 challenged by benthic cyanobacterial mats. *Geobiology* **10**, 371-383.
- 33  
34 637 KLAPPER, G. & BARRICK, J.E. 1978. Conodont ecology: pelagic versus benthic.  
35 638 *Lethaia* **11**, 15-23.
- 36  
37 639 KLAPPER, G. & KIRCHGASSER, W.T. 2016. Frasnian Late Devonian conodont  
38 640 biostratigraphy in New York: graphic correlation and taxonomy. *Journal of*  
39 641 *Paleontology* **90**, 525-554.
- 40  
41 642 KREMER, B. & KAŻMIERCZAK, J. 2005. Cyanobacterial mats from Silurian black  
42 643 radiolarian cherts: phototrophic life at the edge of darkness? *Journal of*  
43 644 *Sedimentary Resarch* **75**, 897-906.
- 44  
45 645 LI TIAN, TONG J., ALGEO, T.J., SONG, H., CHU, D., SHI, L. & BOTTJER, D.J.  
46 646 2014. Reconstruction of Early Triassic ocean redox conditions based on  
47 647 framboidal pyrite from the Nanpanjiang Basin, South China. *Palaeogeography,*  
48 648 *Palaeoclimatology, Palaeoecology* **412**, 68-79.
- 49  
50  
51  
52  
53  
54  
55  
56  
57  
58  
59  
60

- 1  
2  
3 649 Mac LEAN, L.C.W., TYLISZCZAK, T., GILBERT, P.U.P.A., ZHOU, D., PRAY, T.J.,  
4 650 ONSTOTT, T.C. & SOUTHAM, G. 2008. A high-resolution chemical and structural  
5 651 study of framboidal pyrite formed within a low-temperature bacterial biofilm.  
6 652 *Geobiology* **6**, 471-480.
- 7  
8  
9 653 MAHBOUBI, A. & GATOVSKY, Y. 2014. Late Devonian conodonts and event  
10 654 stratigraphy in northwestern Algerian Sahara. *Journal of African Earth Sciences*  
11 655 **101**, 322-332.
- 12  
13  
14 656 MAHBOUBI, A., FEIST, R., CORNÉE, J.-J., MEHADJI, A.O. & GIRARD, C. 2015.  
15 657 Frasnian (Late Devonian) conodonts and environment at the northern margin of  
16 658 the Algerian Sahara platform: the Ben Zireg section. *Geological Magazine* **152**,  
17 659 844-857.
- 18  
19  
20  
21 660 MAMET, B. & PRÉAT, A. 2006. Iron-bacterial mediation in Phanerozoic red  
22 661 limestones: State of the art. *Sedimentary Geology* **185**, 147-157.
- 23  
24 662 MUTTI, E., LUCCHI, F.R., SEGURET, M. & ZANZUCCHI, G. 1984. Seismoturbidites:  
25 663 A new group of resedimented deposits. *Marine Geology* **55**, 103-116.
- 26  
27  
28 664 NARKIEWICZ, M. 1988. Turning points in sedimentary development in the Late  
29 665 Devonian in southern Poland. In *Devonian of the World* (eds McMillan, N.J.,  
30 666 Embry, A.F. & Glass, D.J.). *Canadian Petroleum Geology, Calgary*, 14, 619–636.
- 31  
32  
33 667 PAREYN, C. 1961. Les Massifs Carbonifères du Sahara Sud-Oranais. *Publications*  
34 668 *du Centre de Recherches Sahariennes*, série Géologie, Paris, 1–324.
- 35  
36 669 PAS, D., DA SILVA, A.C., CORNET, P., BULTYNCK, P., KÖNIGSHOF, P. &  
37 670 BOULVAIN, F. 2013. Sedimentary development of a continuous Middle Devonian  
38 671 to Mississippian section from the fore-reef fringe of the Brilon Reef Complex  
39 672 (Rheinisches Schiefergebirge, Germany). *Facies* **59**, 969-990.
- 40  
41  
42  
43 673 PAS, D., DA SILVA, A.C., SUTTER, T., KIDO, E., BULTYNCK, P., PONDRELLI, M.,  
44 674 CORRADINI, C., DEVLEESCHOUWER, X., DOJEN, C. & BOULVAIN, F. 2014a.  
45 675 Insight into the development of a carbonate platform through a multi-disciplinary  
46 676 approach: a case study from the Upper Devonian slope deposits of Mount  
47 677 Freikofel (Carnic Alps, Austria/Italy). *International Journal of Earth Sciences* **103**,  
48 678 519-538.
- 49  
50  
51  
52  
53 679 PAS, D., DA SILVA, A.C., DEVLEESCHOUWER, X., DE VLEESCHOUWER, D.,  
54 680 LABAYE, C., CORNET, P., MICHEL, J., BOULVAIN, F. 2014b. Sedimentary  
55 681 development and magnetic susceptibility evolution of the Frasnian in Western

- 1  
2  
3 682 Belgium (Dinant Synclinorium, La Thure section). *Geological Society of London*,  
4 683 Special Publication **414**, 15-36.
- 5  
6 684 PECKMANN, J. & THIEL, V. 2004. Carbon cycling at ancient methane-seeps.  
7  
8 685 *Chemical Geology* **205**, 443–467.
- 9  
10 686 PETTER, G. 1952. Dévonien moyen et supérieur. In *Les chaines d'Ougarta et la*  
11 687 *Saoura* (eds Alimen, H.D., Le Maitre, D., Menchikoff, N., Petter, G. & Poueyto, A.).  
12 688 19<sup>th</sup> Congrès géologique International, Alger, 62–74.
- 13  
14 689 PETTER, G. 1959. Goniates Dévoniennes du Sahara. Service de la carte  
15 690 géologique de l'Algérie, Alger, 313 pp.
- 16  
17  
18 691 ROSSETTI, D.F. & GÓES, A.M. 2000. Deciphering the sedimentological imprint of  
19 692 paleoseismic events: an example from the Aptian Codó Formation, northern Brazil.  
20 693 *Sedimentary Geology* **135**, 137-156.
- 21  
22  
23 694 SANDBERG, C.A. 1976. Conodont biofacies of Late Devonian *Polygnathus styriatus*  
24 695 Zone in western United States. In *Conodont Paleocology* (ed. C. R. Barnes), pp.  
25 696 171–86. Montreal: Geological Association of Canada, Special Paper no. 15.
- 26  
27  
28 697 SANDBERG, C.A. & ZIEGLER, W. 1979. Taxonomy and biofacies of important  
29 698 conodonts of Late Devonian styriacus Zone, United States and Germany. *Geology*  
30 699 *and Palaeontology*, 13, 173-212.
- 31  
32  
33 700 SANDBERG, C.A., ZIEGLER, W., DREESEN, R. & BUTLER, J.L. 1992. Conodont  
34 701 biochronology, biofacies, taxonomy, and event stratigraphy around middle  
35 702 Frasnian Lion Mudmound (F2h), Frasnies, Belgium. *Courier Forschungsinstitut*  
36 703 *Senckenberg* **150**, 1–87.
- 37  
38  
39 704 SANDBERG, C.A., MORROW, J.R. & ZIEGLER, W. 2002. Late Devonian sea-level  
40 705 changes, catastrophic events, and mass extinctions. *Special papers - Geological*  
41 706 *Society of America*, 473-488.
- 42  
43  
44 707 SCHIEBER, J. 1986. The possible role of benthic microbial mats during the formation  
45 708 of carbonaceous shales in shallow Proterozoic basins. *Sedimentology* **33**, 521-  
46 709 536.
- 47  
48  
49 710 SCHIEBER, J. 1989. Facies and origin of shales from the Mid-Proterozoic Newland  
50 711 Formation, Belt basin, Montana, USA. *Sedimentology* **36**, 203-219.
- 51  
52  
53 712 Schülke, I. & Popp, A. 2005. Microfacies development, sea-level change, and  
54 713 conodont stratigraphy of Famennian mid- to deep platform deposits of the  
55 714 Beringhauser Tunnel section (Rheinisches Schiefergebirge, Germany). *Facies* **50**,  
56 715 647-664.  
57  
58  
59  
60

- 1  
2  
3 716 SEDDON, G. & SWEET, W.C. 1971. An ecologic model for conodonts. *Journal of*  
4 717 *Paleontology* **45**, 869-880.  
5  
6 718 SPALLETTA, C. & VAI, G.B. 1984. Upper Devonian intraclast parabreccias  
7 719 interpreted as seismites. *Marine Geology* **55**, 133-144.  
8  
9 720 SUR, S., SCHIEBER, J. & BANERJEE, S. 2006. Petrographic observations  
10 721 suggestive of microbial mats from Rampur Shale and Bijaigarh Shale, Vindhyan  
11 722 basin, India. *Journal of Earth System Science* **115**, 61-66.  
12  
13 723 WENDT, J. & BELKA, Z. 1991. Age and depositional environment of Upper Devonian  
14 724 (early Frasnian to early Famennian) black shales and limestones (Kellwasser  
15 725 facies) in the eastern Anti-Atlas, Morocco. *Facies* **25**, 51-89.  
16  
17 726 WENDT, J., KAUFMANN, B., BELKA, Z., KLUG, C. & LUBESIEDER, S. 2006.  
18 727 Sedimentary evolution of a Palaeozoic basin and ridge system: the Middle and  
19 728 Upper Devonian of the Ahnet and Mouydir (Algerian Sahara). *Geological*  
20 729 *Magazine* **143**, 269-299.  
21  
22 730 WEYANT, M. 1988. Relationship between Devonian and Carboniferous strata near  
23 731 the northern confines of the Bechar basin, Algeria. *Courier Forschungsinstitut*  
24 732 *Senckenberg* **100**, 235-241  
25  
26 733 WIGNALL, P.B., NEWTON, R. & BROOKFIELD, M.E. 2005. Pyrite framboid  
27 734 evidence for oxygen-poor deposition during the Permian–Triassic crisis in  
28 735 Kashmir. *Palaeogeography, Palaeoclimatology, Palaeoecology* **216**, 183-188.  
29  
30 736 WRIGHT, V. P. & BURCHETTE, T. P. 1996. Shallow-water carbonate environments.  
31 737 In *Sedimentary Environments: Processes, Facies, and Stratigraphy* (ed. H. G.  
32 738 Reading), pp. 325–94. Oxford: Blackwell Science.  
33  
34  
35  
36  
37  
38  
39  
40  
41 739  
42  
43  
44  
45  
46  
47  
48  
49  
50  
51  
52  
53  
54  
55  
56  
57  
58  
59  
60



740

741 **Figure captions**

742 **Fig. 1.** (a) Location of South Marhouma section (Ougarta basin) and Ben Zireg  
743 section (Bechar basin) in NW Algeria (photograph from Google Earth). (b)  
744 Investigated section in the Saoura region (after Petter, 1959). (c) Investigated section  
745 in the Ben Zireg anticline (after Pareyn, 1961).

746

747 **Fig. 2.** Lithological column with relative abundance of fossil components and facies  
748 fabrics of the Ben Zireg section. Conodont zones from Mahboubi et al. (2015).  
749 Lithostratigraphic units: (Unit 1) ochre cherty limestones with soft-deformations, (Unit  
750 2) massive micritic limestones, (Unit 3) ferruginous limestones, (Unit 4) pseudo  
751 nodular argillaceous limestones, (Unit 5) nodular limestones. Abbreviations: Hg, Hard  
752 ground; M, Mudstone; W, Wackestone; P, Packstone; F, Floatstone; FZ, Frasnian  
753 Zone (after Klapper & Kirchgasser, 2016).

754

755 **Fig. 3.** Lithofacies. (a) Convolute laminations (Ben Zireg). (b) Thin-bedded, upper  
756 Frasnian micritic limestones (Ben Zireg). (c) Detail of the Upper Kellwasser bed in the  
757 Ben Zireg section with a thin layer of black shales (red arrow) superseded by  
758 laminated pinkish calcisiltic shale (black arrow). (d) Black shales (Marhouma). (e)  
759 Alternating pseudonodular limestone beds and grey shales (Marhouma section). (f)  
760 Interbedded argillaceous micritic nodules (Marhouma Formation). (g) Upper  
761 Kellwasser bed in the South Marhouma section with laminated black to pinky shales.  
762 (h) Dm-thick diagenetic limestones and black shales from early Famennian strata of  
763 the Marhouma section.

764

765 **Fig. 4.** Lithological column with relative abundance of fossil components and facies  
766 fabrics of the South Marhouma section. Conodont zones from Mahboubi & Gatovsky  
767 (2014). Lithostratigraphic units: (Unit1) dark shales, (Unit 2) bioclastic  
768 nodular/pseudonodular limestones-grey shales, (Unit 3) nodular muddy limestones-  
769 greenish/darkish shales, (Unit 4) Diagenetic limestones/black shales. Abbreviations:  
770 Hg, Hard ground; M, Mudstone; W, Wackestone; P, Packstone, *L.tr.*, Lower  
771 *triangularis*; FAM, Famennian; FZ, Frasnian Zone.

772

1  
2  
3 773 **Fig. 5.** Facies of the depositional environments of the South Marhouma section and  
4 the Ben Zireg section. Scale (yellow bar) is 1mm. (a) Facies F2, outer ramp deposit:  
5 774 reworked mudstone layers in the Ben Zireg section (bed BZ2B). (b) ) Facies F2,  
6 775 outer ramp deposit: microscopic view (bed BZ1C). (c) Facies F6, mid-outer ramp  
7 776 deposit: lime mudstone with cephalopod bioclasts (bed MH34. (d) Facies F4, outer  
8 777 ramp deposit: pelagic argillaceous wackstone displaying distinct lamination by  
9 778 parallel arrangement of tentaculite coquinas (bed MH10). (e) Facies F6, outer ramp  
10 779 deposit: diversified wackestone with bioclasts consisting of abundant brachiopod  
11 780 shells (bed MH32). (f) ) Facies F6, mid ramp deposit: fine-grained mudstone with  
12 781 benthic ostracods (bed BZ10B). Abbreviations: br, brachiopod; go, goniatite; ort,  
13 782 orthoceras; os, ostracod; pa, parabreccia; ra, radiolarian; tr, trilobite; te, tentaculite  
14 783  
15 784

16  
17  
18  
19  
20  
21  
22  
23 785 **Fig. 6.** Facies F7, mid ramp deposits, latest Frasnian at South Marhouma and Ben  
24 786 Zireg sections. (a) Flat-pebble conglomerate fabric (bed MH26bas). (b) SEM image  
25 787 of kerogenous laminae (wavy-crinkly structures) (bed MH29). (c, e) Kerogenous  
26 788 laminae. Note that these structures are more abundant in the South Marhouma  
27 789 samples (picture b, bed MH29) compared to the Ben Zireg sample (picture e, bed  
28 790 BZ15D). (d) SEM image of tube-like structures (black arrows, bed BZ15D) associated  
29 791 with framboidal pyrite (white arrow). (f) Finely-laminated striped shale displaying  
30 792 graded silt-mud couplets (bed MH30).  
31 793  
32 794

33 795 **Fig. 7.** Sedimentary model in NW Algeria during the Frasnian period (South  
34 796 Marhouma and Ben Zireg sections). This model shows a mid to outer ramp setting  
35 797 with lateral distribution of facies from the most proximal setting (F7) to the the most  
36 798 distal (F1). SWB, Storm Wave-Base; FWWB, Fair Weather Wave-Base.  
37 799  
38 800

39 801 **Fig. 8.** Magnetic susceptibility evolution, facies change, and sea-level fluctuations  
40 802 through the Frasnian in the South Marhouma section. FZ: Frasnian Zones, LKW:  
41 803 Lower Kellwasser, UKW: Upper Kellwasser.  
42  
43  
44  
45  
46  
47  
48  
49  
50  
51  
52  
53  
54  
55  
56  
57  
58  
59  
60

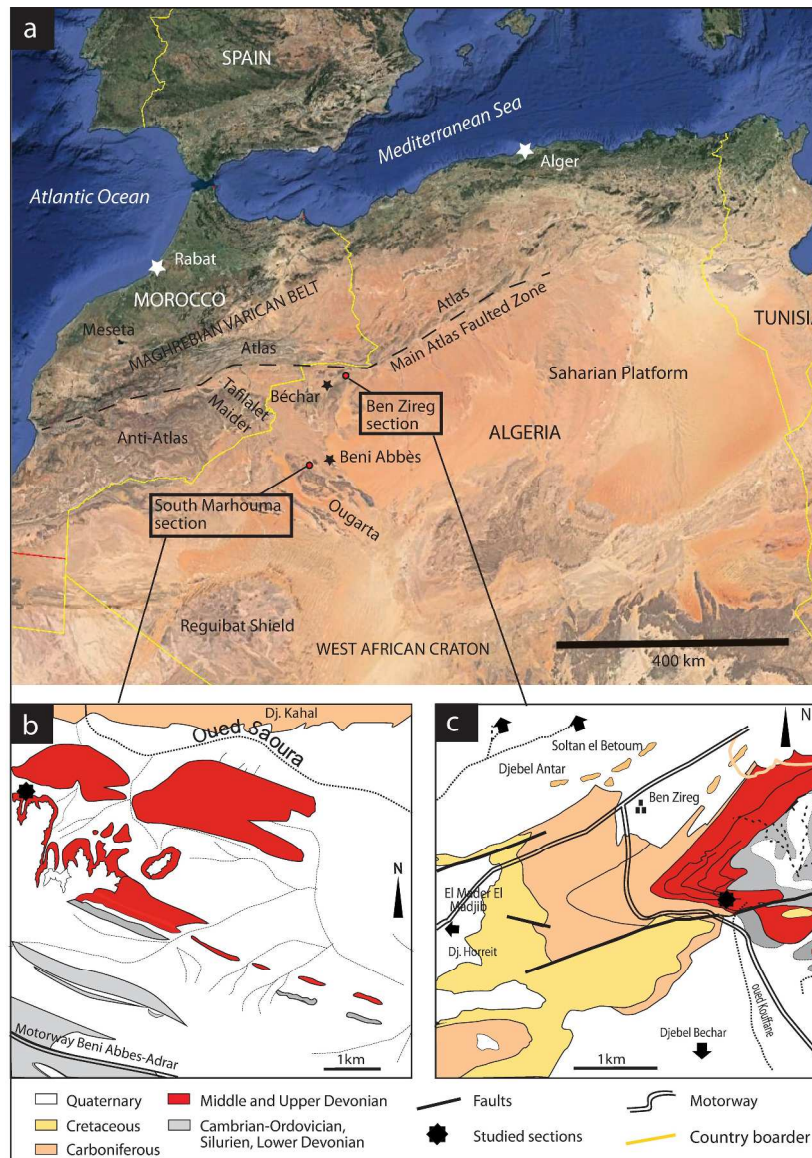
1  
2  
3 804 **Fig. 9.** Magnetic susceptibility evolution, facies change, and sea-level fluctuations  
4  
5 805 through the Frasnian in the Ben Zireg section. FZ: Frasnian Zones, LKW: Lower  
6  
7 806 Kellwasser, UKW: Upper Kellwasser.  
8

9 807

10 808

11  
12 809 **Fig. 10.** Comparison of sea-level fluctuations from Euramerica and North Africa  
13  
14 through the Frasnian stage. FZ (Frasnian Zones) after Klapper & Kirchgasser (2016),  
15  
16 810 relative duration of conodont Zones are from Becker, Gradstein & Hammer (2012). In  
17  
18 811 grey anoxic events. UKW: Upper Kellwasser; LKW: Lower Kellwasser; FAM:  
19  
20 812  
21  
22 813 Famennian.  
23  
24  
25  
26  
27  
28  
29  
30  
31  
32  
33  
34  
35  
36  
37  
38  
39  
40  
41  
42  
43  
44  
45  
46  
47  
48  
49  
50  
51  
52  
53  
54  
55  
56  
57  
58  
59  
60

1  
2  
3  
4  
5  
6  
7  
8  
9  
10  
11  
12  
13  
14  
15  
16  
17  
18  
19  
20  
21  
22  
23  
24  
25  
26  
27  
28  
29  
30  
31  
32  
33  
34  
35  
36  
37  
38  
39  
40  
41  
42  
43  
44  
45  
46  
47  
48  
49  
50  
51  
52  
53  
54  
55  
56  
57  
58  
59  
60



Mahboubi et al., Fig. 1

Fig. 1. (a) Location of South Marhouma section (Ougarta basin) and Ben Zireg section (Bechar basin) in NW Algeria (photograph from Google Earth). (b) Investigated section in the Saoura region (after Petter, 1959). (c) Investigated section in the Ben Zireg anticline (after Pareyn, 1961).

290x408mm (300 x 300 DPI)

Mahboubi\_et\_al\_Fig 2

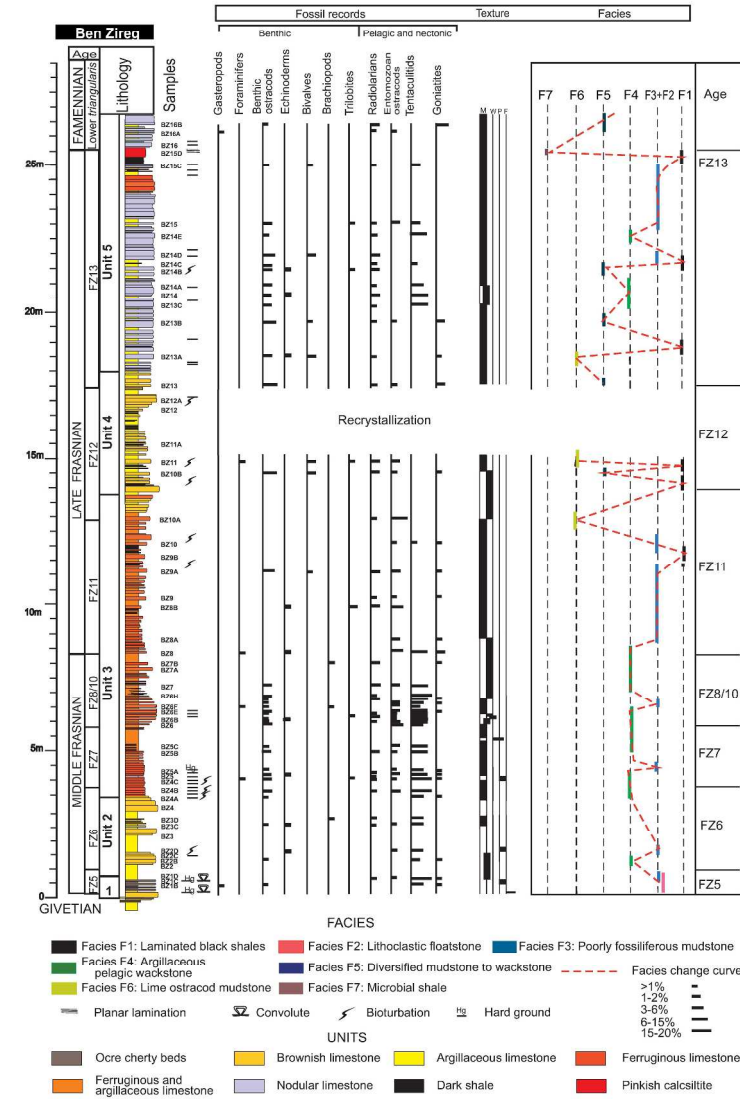


Fig. 2. Lithological column with relative abundance of fossil components and facies fabrics of the Ben Zireg section. Conodont zones from Mahboubi et al. (2015). Lithostratigraphic units: (Unit 1) ochre cherty limestones with soft-deformations, (Unit 2) massive micritic limestones, (Unit 3) ferruginous limestones, (Unit 4) pseudo nodular argillaceous limestones, (Unit 5) nodular limestones. Abbreviations: Hg, Hard ground; M, Mudstone; W, Wackestone; P, Packstone; F, Floatstone; FZ, Frasnian Zone (after Klapper & Kirchgasser, 2016).

283x463mm (300 x 300 DPI)

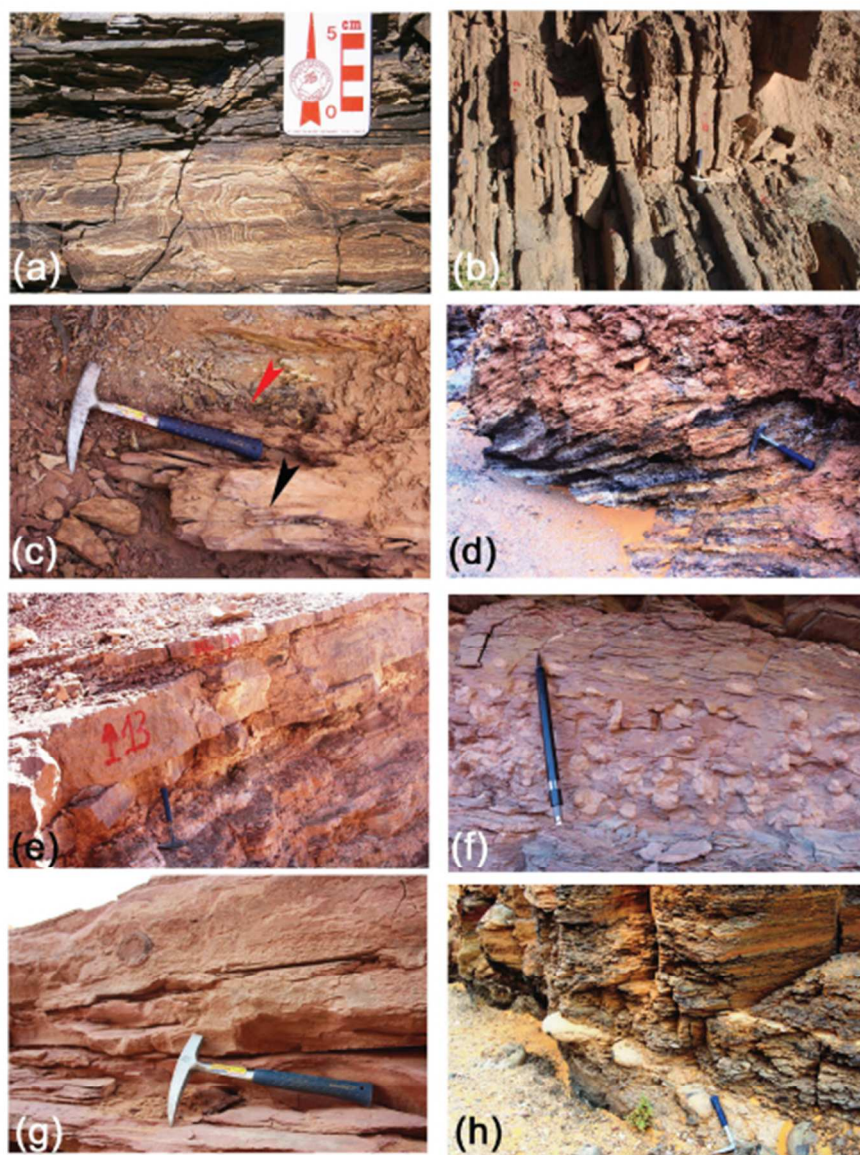
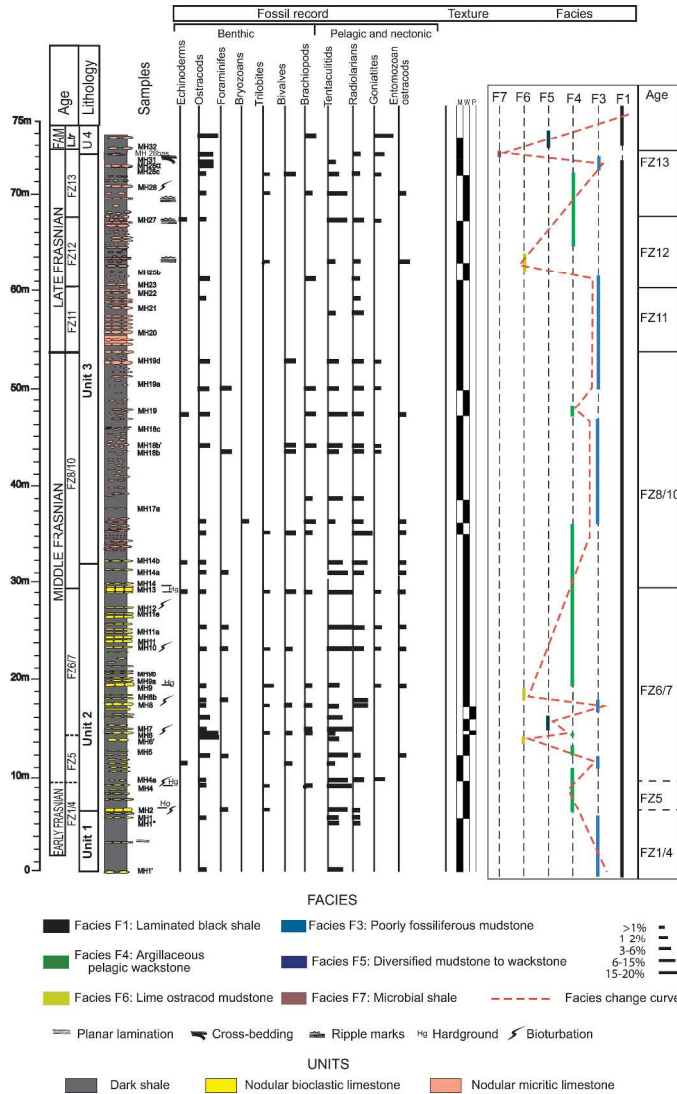


Fig. 3. Lithofacies. (a) Convolute laminations (Ben Zireg). (b) Thin-bedded, upper Frasnian micritic limestones (Ben Zireg). (c) Detail of the Upper Kellwasser bed in the Ben Zireg section with a thin layer of black shales (red arrow) superseded by laminated pinkish calcisiltic shale (black arrow). (d) Black shales (Marhouma). (e) Alternating pseudonodular limestone beds and grey shales (Marhouma section). (f) Interbedded argillaceous micritic nodules (Marhouma Formation). (g) Upper Kellwasser bed in the South Marhouma section with laminated black to pinky shales. (h) Dm-thick diagenetic limestones and black shales from early Famennian strata of the Marhouma section.

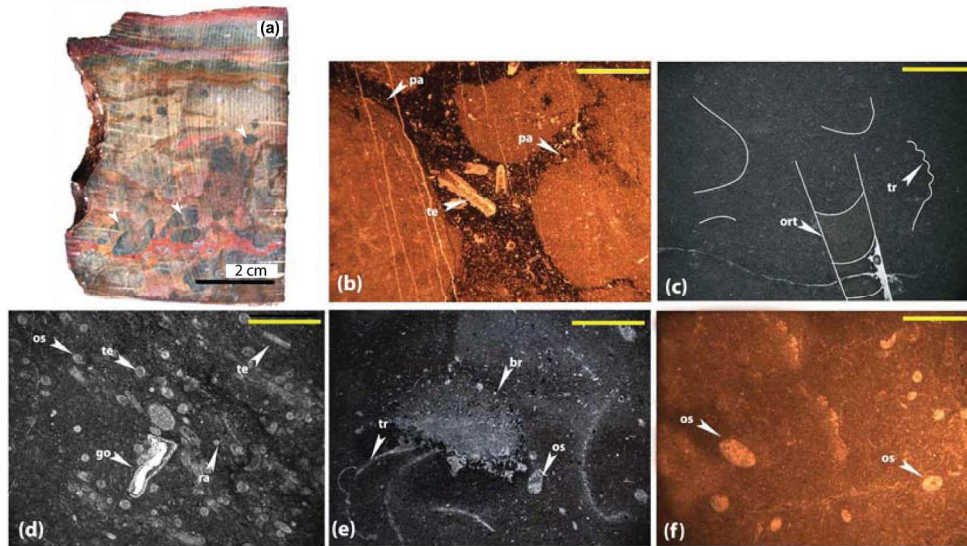
190x239mm (72 x 72 DPI)



Mahboubi et al., Fig. 4

Fig. 4. Lithological column with relative abundance of fossil components and facies fabrics of the South Marhouma section. Conodont zones from Mahboubi & Gatovsky (2014). Lithostratigraphic units: (Unit1) dark shales, (Unit 2) bioclastic nodular/pseudonodular limestones-grey shales, (Unit 3) nodular muddy limestones-greenish/darkish shales, (Unit 4) Diagenetic limestones/black shales. Abbreviations: Hg, Hard ground; M, Mudstone; W, Wackestone; P, Packstone, L.tr., Lower triangularis; FAM, Famennian; FZ, Frasnian Zone.

270x439mm (300 x 300 DPI)

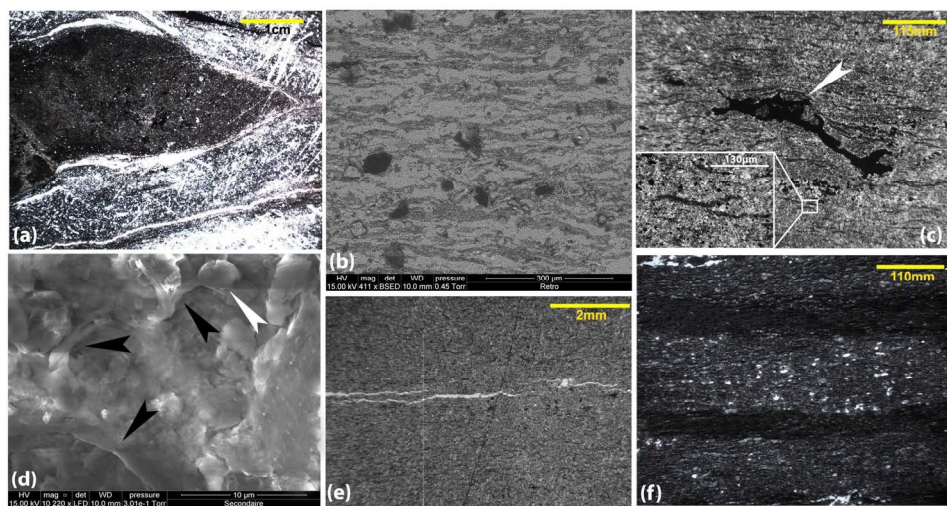


Mahboubi et al. Fig. 5

Fig. 5. Facies of the depositional environments of the South Marhouma section and the Ben Zireg section. Scale (yellow bar) is 1mm. (a) Facies F2, outer ramp deposit: reworked mudstone layers in the Ben Zireg section (bed BZ2B). (b) Facies F2, outer ramp deposit: microscopic view (bed BZ1C). (c) Facies F6, mid-outer ramp deposit: lime mudstone with cephalopod bioclasts (bed MH34). (d) Facies F4, outer ramp deposit: pelagic argillaceous wackestone displaying distinct lamination by parallel arrangement of tentaculite coquinas (bed MH10). (e) Facies F6, outer ramp deposit: diversified wackestone with bioclasts consisting of abundant brachiopod shells (bed MH32). (f) Facies F6, mid ramp deposit: fine-grained mudstone with benthic ostracods (bed BZ10B). Abbreviations: br, brachiopod; go, goniatite; ort, orthoceras; os, ostracod; pa, parabreccia; ra, radiolarian; tr, trilobite; te, tentaculite

167x148mm (300 x 300 DPI)





Mahboubi et al., fig. 6

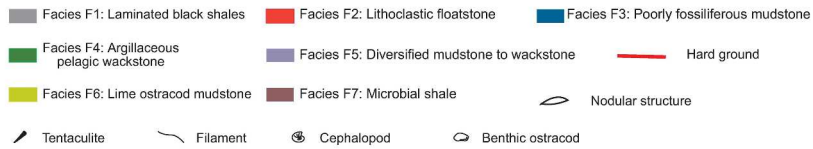
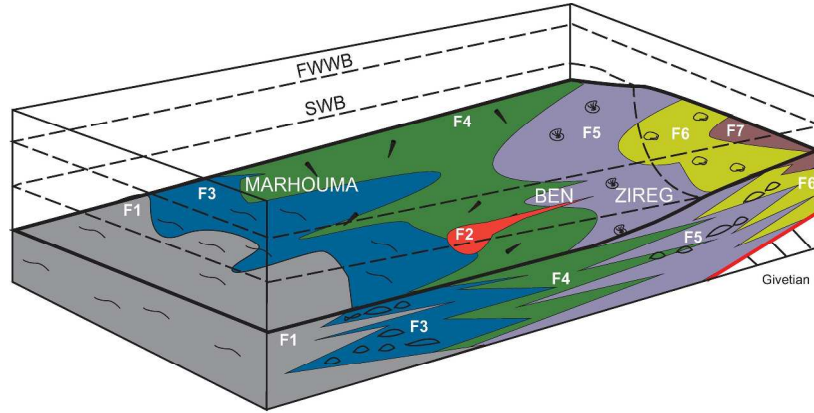
Fig. 6. Facies F7, mid ramp deposits, latest Frasnian at South Marhouma and Ben Zireg sections. (a) Flat-pebble conglomerate fabric (bed MH26bas). (b) SEM image of kerogenous laminae (wavy-crenulate structures) (bed MH29). (c, e) Kerogenous laminae. Note that these structures are more abundant in the South Marhouma samples (picture b, bed MH29) compared to the Ben Zireg sample (picture e, bed BZ15D). (d) SEM image of tube-like structures (black arrows, bed BZ15D) associated with framboidal pyrite (white arrow). (f) Finely-laminated striped shale displaying graded silt-mud couplets (bed MH30).

168x133mm (300 x 300 DPI)

SEM

1  
2  
3  
4  
5  
6  
7  
8  
9  
10  
11  
12  
13  
14  
15  
16  
17  
18  
19  
20  
21  
22  
23  
24  
25  
26  
27  
28  
29  
30  
31  
32  
33  
34  
35  
36  
37  
38  
39  
40  
41  
42  
43  
44  
45  
46  
47  
48  
49  
50  
51  
52  
53  
54  
55  
56  
57  
58  
59  
60

1  
2  
3  
4  
5  
6  
7  
8  
9  
10  
11  
12  
13  
14  
15  
16  
17  
18  
19  
20  
21  
22  
23  
24  
25  
26  
27  
28  
29  
30  
31  
32  
33  
34  
35  
36  
37  
38  
39  
40  
41  
42  
43  
44  
45  
46  
47  
48  
49  
50  
51  
52  
53  
54  
55  
56  
57  
58  
59  
60

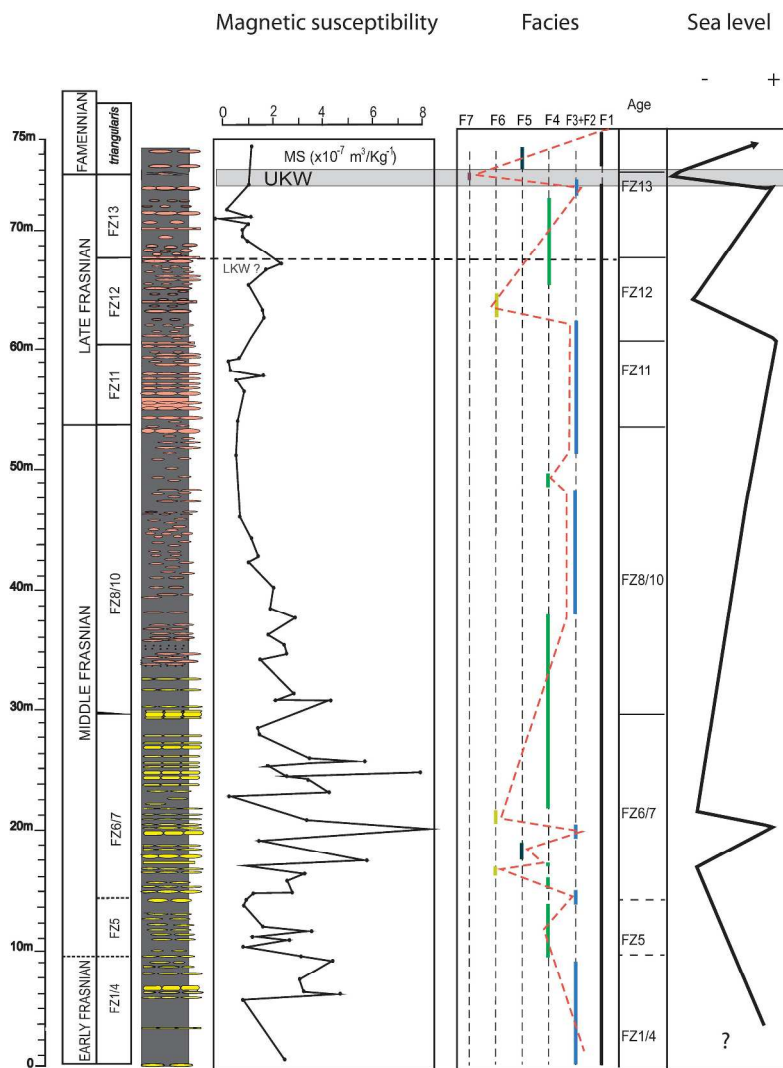


Mahboubi et al. Fig. 7

Mahboubi et al. Fig. 7

Fig. 7. Sedimentary model in NW Algeria during the Frasnian period (South Marhouma and Ben Zireg sections). This model shows a mid to outer ramp setting with lateral distribution of facies from the most proximal setting (F7) to the the most distal (F1). SWB, Storm Wave-Base; FWWB, Fair Weather Wave-Base.

257x378mm (300 x 300 DPI)

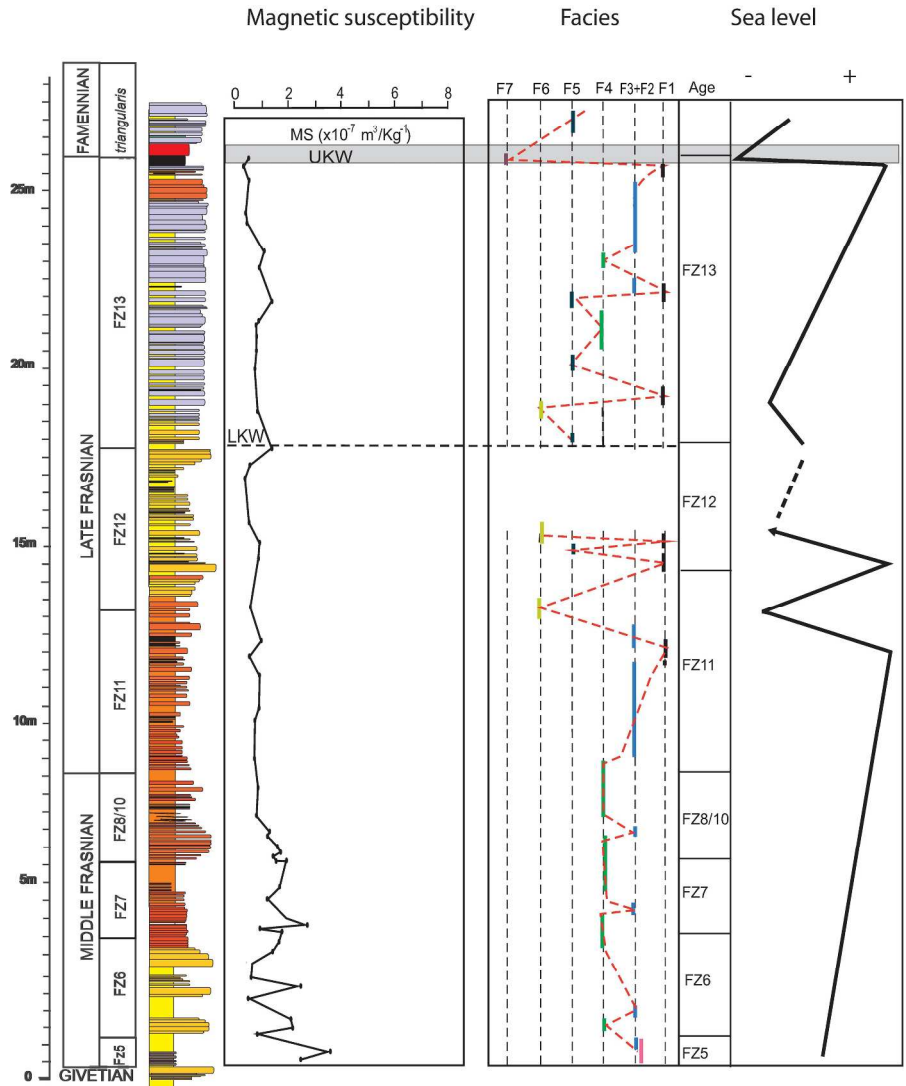


Mahboubi et al., Fig. 8

Fig. 8. Magnetic susceptibility evolution, facies change, and sea-level fluctuations through the Frasnian in the South Marhouma section. FZ: Frasnian Zones, LKW: Lower Kellwasser, UKW: Upper Kellwasser.

260x384mm (300 x 300 DPI)

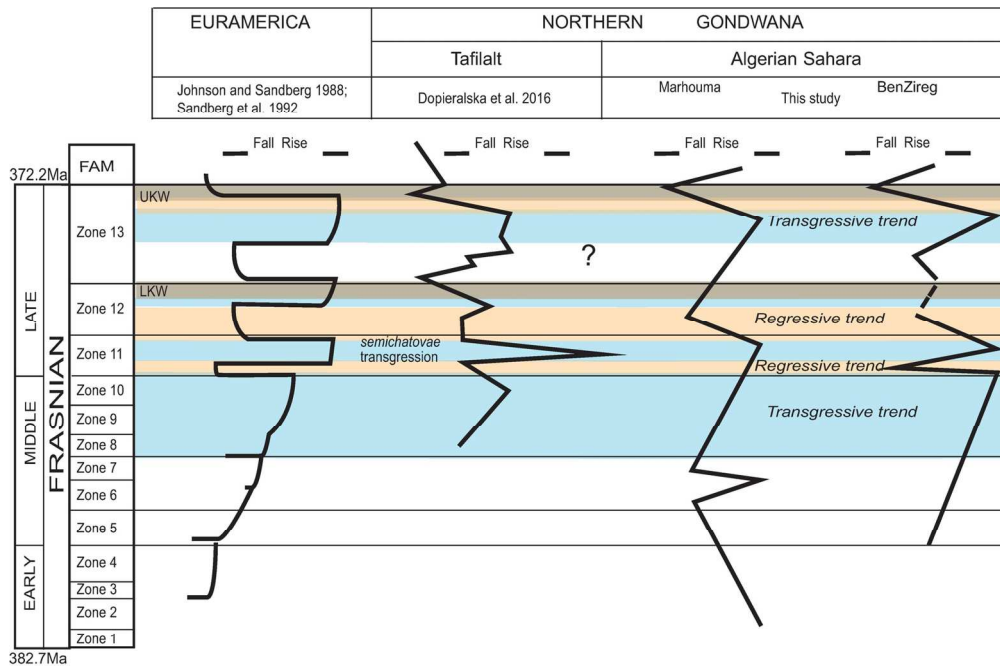
1  
2  
3  
4  
5  
6  
7  
8  
9  
10  
11  
12  
13  
14  
15  
16  
17  
18  
19  
20  
21  
22  
23  
24  
25  
26  
27  
28  
29  
30  
31  
32  
33  
34  
35  
36  
37  
38  
39  
40  
41  
42  
43  
44  
45  
46  
47  
48  
49  
50  
51  
52  
53  
54  
55  
56  
57  
58  
59  
60



Mahboubietal.Fig.9

Fig. 9. Magnetic susceptibility evolution, facies change, and sea-level fluctuations through the Frasnian in the Ben Zireg section. FZ: Frasnian Zones, LKW: Lower Kellwasser, UKW: Upper Kellwasser.

238x320mm (300 x 300 DPI)



Mahboubi et al., Fig.10

Fig. 10. Comparison of sea-level fluctuations from Euramerica and North Africa through the Frasnian stage. FZ (Frasnian Zones) after Klapper & Kirchgasser (2016), relative duration of conodont Zones are from Becker, Gradstein & Hammer (2012). In grey anoxic events. UKW: Upper Kellwasser; LKW: Lower Kellwasser; FAM: Famennian.

147x123mm (300 x 300 DPI)



1  
2  
3  
4  
5  
6  
7  
8  
9  
10  
11  
12  
13  
14  
15  
16  
17  
18  
19  
20  
21  
22  
23  
24  
25  
26  
27  
28  
29  
30  
31  
32  
33  
34  
35  
36  
37  
38  
39  
40  
41  
42  
43  
44  
45  
46  
47  
48  
49  
50  
51  
52  
53  
54  
55  
56  
57  
58  
59  
60